

Investigation of Interface Oil Insufficiency in a Strain Gauge Type Pressure Sensor

Kamran Soltani^{1,*}, Ghader Rezazadeh^{1,2}, Manus Henry^{2,3}, Oleg Bushuev²

¹ Mechanical Engineering Department, Urmia University, Urmia, Iran

² South Ural State University, Chelyabinsk, Russian Federation

³ Department of Engineering Science, Oxford University, Oxford, GB

* **Corresponding Author:** Kamran Soltani (kamransoltani16377@gmail.com)

Abstract

Strain gauge type pressure sensors are widely used in different branches of industry to measure pressure from very low to very high (1400 Mpa) values. This article investigates a strain gauge type pressure sensor that uses silicon oil within its housing to transmit working pressure from the external environment to a sensing plate. An important failure mode arises from loss/leakage of the silicon oil, whereby a portion of the internal volume is replaced by gas, usually air. Coupled nonlinear governing equations have been derived and solved in both static and dynamical states to describe the behavior of the external membrane, the interface oil including pockets of gas, and the sensing plate. Nonlinear behavior arises from the plate and membrane midplane stretching, and of course the behavior of the gas. The resulting model describes how oil loss affects the sensor performance and changes the sensor output and pressure measurable range.

Keywords: Pressure sensor; Strain gauge; Oil leakage; Oil insufficiency; Non-linear behavior.

1 Introduction

Accurate measurement of pressure plays a key role in many applications such as automotive, industrial, aerospace, biomedical, etc. Accordingly, pressure sensors play a pivotal role in such systems [1]–[4]. Manometers, bourdon tubes, and diaphragms were among the first generation of pressure sensing technology, based on converting pressure into the mechanical movement of an indicator [5].

The subsequent development of pressure measurement technology led to the creation of electro-mechanical pressure transducers in which the input pressure is directly converted into an electrical signal [5]–[8]. It is useful to draw the widely-used distinction between the primary sensing element, the transducer, which generates an initial signal (usually electrical) directly from the property being measured (here pressure), and the transmitter, which includes the additional elements (process interface, housing, signal conditioning, analog-to-digital conversion, processing software, linearization, external communication) to implement the complete measurement task. The term ‘sensor’ can generally be interpreted to mean either the transducer or the transmitter; in this paper, only the transduction of pressure to an initial electrical signal is considered, and so the terms sensor and transducer are used interchangeably.

Today, the most commonly used pressure transducers are piezo or tenso-resistive (or strain gauge) [5], [6], [9], [10], capacitive [2], [11]–[13], and piezoelectric [14], [15]. Each of these pressure transducer types operates on simple physical properties and have their special own

capabilities. Capacitive pressure sensors are based on detecting a change in capacitance due to proportionally applied pressure. In piezoelectric transducers, the piezoelectric effect is a property of certain materials whereby an electrical charge is generated when mechanical stress is applied; this effect is a reversible process [5], [6], [9], [11]. Piezoresistive transducers have several advantages over other pressure sensing technologies, such as high sensitivity, low cost, small size, and an easy fabrication process, so that they are the most widely used in pressure measurement applications [6]. They and their corresponding transmitters may be further classified in various ways, including the material used for piezo-resistors [16], [17], the material used to build diaphragms [16], [18], [19], the wafer type [20], the method of micromachining the diaphragm [18] as well as the type of pressure to be measured (absolute, gauge, differential). A useful literature review of design principles and considerations for piezoresistive pressure transducers and transmitters is provided by Kumar et.al. [6].

In piezoresistivity, the transducer resistance changes due to strain caused by mechanical loading. This characteristic is used in many measuring devices including pressure sensors, accelerometers, inertial sensors, strain gauges, and cantilever force sensors [21]. A piezoresistive pressure transducer typically consists of a diaphragm or a plate that is deflected proportionally to the applied pressure. In some piezoresistive transducers, the pressure applied by the industrial process to the external diaphragm is transferred to a stiffer plate via an interface fluid such as silicon oil. This design typically restricts the maximum deflection of the diaphragm in order to prevent mechanical degradation. Figure 1 shows a schematic view of this type of pressure sensor. The plate (lower diaphragm) includes strain gauges to measure the deformation by converting it to an electrical output signal. The fluid in the cavity between the two diaphragms (the interface volume) is by design incompressible. Any compressibility of the fluid will result in an incomplete transfer of pressure to the lower plate as energy is expended in compressing the fluid. This in turn leads to errors in the resulting pressure measurement.

An important failure mode for pressure sensors of this type can occur when the transducer is not completely full of the incompressible fluid. This may arise due to incomplete filling during the fabrication process, or as a result of a leakage arising from mechanical damage. This condition may result in disruption of the measurement performance of the pressure sensor. The authors have not been able to discover previous work examining this condition. This paper shows an analytical and numerical approach for modeling oil insufficiency in a strain gauge type pressure sensor in both static and dynamic cases, respectively. The air between the two diaphragms is modeled as an ideal gas. Also, the initial deflections of the membrane and sensing is investigated to determine the change in the pressure range measured by this sensor. The nonlinear governing equations to the system are obtained and solved, and the influence of an air layer on the sensor's performance is studied in the following sections.

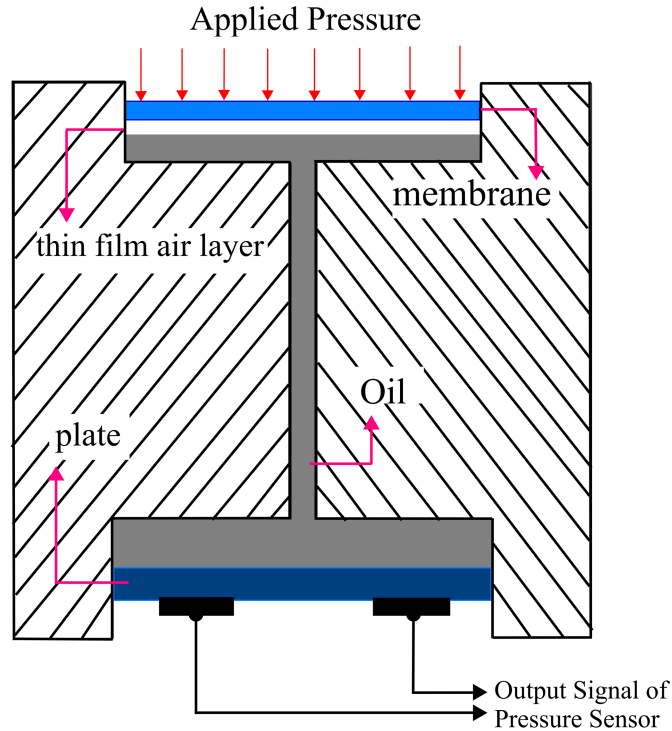


Fig.1: Cross-sectional view of the investigated pressure sensor.

2 Modeling

A schematic view of a strain gauge pressure sensor is shown in Fig. (1). The sensor comprises three main components, the upper diaphragm or isolator membrane, the lower diaphragm or plate, on which the strain gauge sensors are installed, and the interface fluid which transfers the applied pressure from the membrane to the plate. In an ideal case, the interface volume between two plates is filled with an incompressible fluid such as silicon oil. However, in some cases, this interface volume is filled with a mixture of oil and gas (in this study the air and gas are equivalent), which causes the behavior of the interface liquid to be compressible and affects the performance of the transducer. In this study, it is considered that the air bubbles in the oil are combined and form a thin layer of air inside the pressure sensor. Also, should be mentioned that the content investigated here may generalize to any other gas that obeys the ideal gas law. This paper deals with the static and dynamic investigation of the sensor under a pressure applied to the membrane. Given the uniform pressure distribution on the membrane as well as on the plate, it can be assumed that the deformation of the membrane and plate is only a function of their radial characteristics, therefore, the problem can be modeled as axisymmetric.

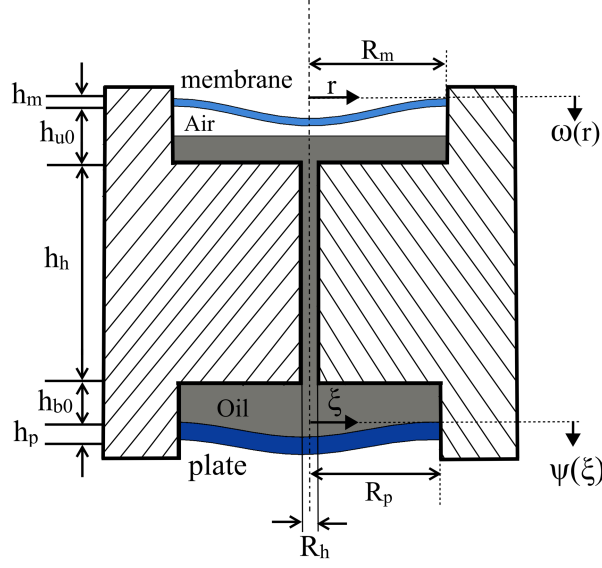


Fig.2: A schematic view of the pressure sensor under an applied pressure P_{in} on the membrane.

Figure (2) introduces the main variables of the model, from which the following equations can be derived in the general dynamic form [10], [22], [23]:

$$D_m \nabla^4 w - \frac{E_m h_m}{1 - \nu_m^2} \left(\frac{1}{2} \int_0^{R_m} \left(\frac{\partial w}{\partial r} \right)^2 dr \right) \nabla^2 w + \rho_m h_m \frac{\partial^2 w}{\partial t^2} + C_m \frac{\partial w}{\partial t} = \hat{P}_{in}(t) - \hat{P}_{Gas}(t) \quad (1)$$

$$D_p \nabla^4 \psi - \frac{E_p h_p}{1 - \nu_p^2} \left(\frac{1}{2} \int_0^{R_p} \left(\frac{\partial \psi}{\partial \xi} \right)^2 d\xi \right) \nabla^2 \psi + \rho_p h_p \frac{\partial^2 \psi}{\partial t^2} + C_p \frac{\partial \psi}{\partial t} = \hat{P}_{Gas}(t) - \hat{P}_{atm} \quad (2)$$

$$\hat{P}_{Gas}(t) V_{Gas}(t) = n \bar{R} T_{Gas} \quad (3)$$

where ∇^2 and $\nabla^4 = \Delta^2$ are Laplacian and bi-Laplacian operator respectively and, for axisymmetric conditions, can be expressed as follows:

$$\nabla^2 = \frac{\partial^2}{\partial r^2} + \frac{1}{r} \frac{\partial}{\partial r}, \quad \nabla^4 = \frac{\partial^4}{\partial r^4} + \frac{2}{r} \frac{\partial^3}{\partial r^3} - \frac{1}{r^2} \frac{\partial^2}{\partial r^2} + \frac{1}{r^3} \frac{\partial}{\partial r} \quad (4)$$

Here w and ψ are the transverse displacement of the membrane and the plate, respectively. r and ξ denote the radial position of the membrane and plate respectively. \hat{P}_{Gas} is the absolute pressure of the gas, V_{Gas} is the gas volume, T_{Gas} is the gas temperature, n is the number of moles of air and \bar{R} , is the universal gas constant. $D_m = \frac{E_m h_m^3}{12(1-\nu_m^2)}$, and $D_p = \frac{E_p h_p^3}{12(1-\nu_p^2)}$ are the flexural rigidity of the membrane and plate respectively, where E , h and ν represent Young's modulus, the diaphragm thickness, and Poisson's ratio. R_m and R_p are the membrane and plate radiuses, respectively. C_m and C_p are equivalent damping on the membrane and sensing plate, respectively. The second terms of the left-hand side of equations (1) and (2) represent the midplane stretching. Midplane stretching is negligible for small deflections of the membrane and plate, however, it can be significant for large deflections. Equation (3) is the time-varying

ideal gas state equation that relates the gas pressure to its volume and temperature. The boundary conditions for governing equations (1) and (2) arise from the fact that the plate and membrane must both be fixed or clamped at the edges so that the deflection and slope are zero at the boundary. So, mathematically, boundary and initial conditions are expressed as follows:

$$\begin{aligned} w(R_m) = \frac{\partial w}{\partial r} \Big|_{r=R_m} &= 0, \quad \psi(R_p) = \frac{\partial \psi}{\partial \xi} \Big|_{\xi=R_p} = 0 \\ w(r, 0) = \frac{\partial w}{\partial t} \Big|_{t=0} &= 0, \quad \psi(\xi, t) = \frac{\partial \psi}{\partial t} \Big|_{t=0} = 0 \end{aligned} \quad (5)$$

Besides, the solution for $w(r, t)$ and $\psi(\xi, t)$ should be finite at all points in the solution domain. Here we investigate the air layer in the interface volume, but the analysis can be applied for any gas that follows the ideal gas law. In the absence of any input gauge pressure applied to the membrane, the volume of air is denoted by $V_{Gas}^{(0)}$, while for an input absolute pressure P_{in} ($P_{in}(t) = P_{gauge}(t) + P_{atm}$) the volume of air changes to V . The volume changes of the gas are also dependent upon the deflection values of the plate and membrane so that in an isothermal condition the relationship can be expressed as follows:

$$V_{Gas}(t) = V_{Gas}^{(0)} - \Delta V(t) = V_{Gas}^{(0)} - (\Delta V_m(t) - \Delta V_p(t)) \quad (6)$$

$$\begin{aligned} &= V_{Gas}^{(0)} - \left(\int_0^{2\pi} \int_0^{R_m} w(r, t) r dr d\theta - \int_0^{2\pi} \int_0^{R_p} \psi(\xi, t) \xi d\xi d\theta \right) \\ V_{Gas} &= V_{Gas}^{(0)} - 2\pi \left(\int_0^{R_m} w(r, t) r dr - \int_0^{R_p} \psi(\xi, t) \xi d\xi \right), \quad V_{Gas}^{(0)} = \pi R_m^2 g_{Gas}^{(0)} \end{aligned} \quad (7)$$

where g_{Gas} , is the equivalent thickness of the gas film. $\Delta V_m(t)$ and $\Delta V_p(t)$ are the variations of the interface volume related to the membrane and plate deflections, respectively. Putting equation (7) into equation (3) the ideal gas state equation takes the following form:

$$\hat{P}_{Gas}(t) \left(V_{Gas}^{(0)} - 2\pi \left(\int_0^{R_m} w(r, t) r dr - \int_0^{R_p} \psi(\xi, t) \xi d\xi \right) \right) = n \bar{R} T_{Gas} \quad (8)$$

Substituting \hat{P}_{Gas} from equation (8) into equations (2) and (3) the differential equations of the membrane and plate static deflections in term of applied pressure can be written as:

$$\begin{aligned} D_m \nabla^4 w - \frac{E_m h_m}{1 - \nu_m^2} \left(\frac{1}{2} \int_0^{R_m} \left(\frac{\partial w}{\partial r} \right)^2 dr \right) \nabla^2 w + \rho_m h_m \frac{\partial^2 w}{\partial t^2} \\ = - \frac{n \bar{R} T_{Gas}}{V_{Gas}^{(0)} - 2\pi \left(\int_0^{R_m} w(r, t) r dr - \int_0^{R_p} \psi(\xi, t) \xi d\xi \right)} + \hat{P}_{in} \end{aligned} \quad (9)$$

$$D_p \nabla^4 \psi - \frac{E_p h_p}{1 - \nu_p^2} \left(\frac{1}{2} \int_0^{R_p} \left(\frac{\partial \psi}{\partial \xi} \right)^2 d\xi \right) \nabla^2 \psi + \rho_p h_p \frac{\partial^2 \psi}{\partial t^2} = \frac{n \bar{R} T_{Gas}}{V_{Gas}^{(0)} - 2\pi \left(\int_0^{R_m} w(r, t) r dr - \int_0^{R_p} \psi(\xi, t) \xi d\xi \right)} - \hat{P}_{atm} \quad (10)$$

As can be seen, equations (9) and (10) are nonlinear and coupled equations. Solving these equations for a given input pressure provides the sensing plate deformation as a mechanical output signal. It is worth mentioning that $g_{Gas}^{(0)}$ used here is an equivalent thickness of the air layer, because in practice the air may be distributed at multiple sites within the interface volume.

3 Numerical Analysis

Given the nonlinearity in the governing equations introduced by the gas pressure and mid-plane stretching terms, the development of an analytical solution is not practical, and therefore we must use a numerical method for solving the governing equations of the system. A well-defined linear equation has a unique solution whereas a nonlinear one can have more than one solution. However, some of the solutions of a nonlinear system could be imaginary or physically impossible and some of them could be physically possible but unstable.

Accordingly, the accuracy and reliability of the solution depends strongly on the selection of a suitable numerical method. One of the most widely applied numerical methods for solving nonlinear systems is by linearizing the nonlinear terms about a known point of the system, but this method can introduce significant errors, especially when the system has large variation around the selected point. Here the numerical analysis is divided into two main subsection 1) static and dynamic analysis.

3.1 Static Analysis

In the static analysis the time dependent terms in equations (9) and (10) are eliminated. To overcome the difficulties non-linearity of the equations the linearization strategy is used. Here, in order to reduce the errors introduced by linearization, a step-by-step linearization method (SSLM) is used. Details are discussed in [24]. Note that we retain the assumption that the temperature is constant. To assist in simplifying the form of the equations, the following definitions are introduced:

$$NT = \frac{n \bar{R} T_{Gas}}{V_{Gas}^{(0)} - 2\pi \left(\int_0^{R_m} w(r) r dr - \int_0^{R_p} \psi(\xi) \xi d\xi \right)}, \quad T = \nabla^2, \quad L = \nabla^4 \quad (11)$$

Assuming a known condition at step k for an input pressure, \bar{p}_{in}^k , parameter values can be calculated for step $k + 1$ as following:

$$w^{k+1} = w^k + \delta w = w^k + \phi(r), \quad \psi^{k+1} = \psi^k + \delta \psi = \psi^k + \gamma(\xi) \quad (12)$$

when the pressure is increased as follows:

$$\hat{P}_{in}^{k+1} = \hat{P}_{in}^k + \Delta \hat{P}_{in} \quad (13)$$

Considering the above relationships and definitions, differential equations (9) and (10) at step $k + 1$ can be rewritten as follows:

$$\begin{cases} D_m L(w^{k+1}) - N_{am}^{k+1} T(w^{k+1}) = -NT^{k+1} + \hat{P}_{in}^{k+1} \\ D_p L(\psi^{k+1}) - N_{ap}^{k+1} T(\psi^{k+1}) = -NT^{k+1} + \hat{P}_{atm} \end{cases} \quad (14)$$

where the axial stretching forces are calculated as follows:

$$N_{am}^{k+1} = \frac{E_m h_m}{2(1 - v_m^2)} \int_0^{R_m} \left(\frac{\partial w^{k+1}}{\partial r} \right)^2 dr \quad (15)$$

$$N_{ap}^{k+1} = \frac{E_p h_p}{2(1 - v_p^2)} \int_0^{R_p} \left(\frac{\partial \psi^{k+1}}{\partial \xi} \right)^2 d\xi \quad (16)$$

Noting that L and T are linear operators they can be expanded as follows:

$$\begin{aligned} L(w^{k+1}) &= L((w^k) + \phi(r)) = L(w^k) + L(\phi(r)), T(w^{k+1}) \\ &= T(w^k) + T(\phi(r)) \\ L(\psi^{k+1}) &= L(\psi^k) + L(\gamma(\xi)), T(\psi^{k+1}) = T(\psi^k) + T(\gamma(\xi)) \end{aligned} \quad (17)$$

for the nonlinear term on the right-hand side in step $k + 1$ we have:

$$NT^{k+1} = \frac{n\bar{R}T_{Gas}}{V_{Gas}^{(0)} - 2\pi \left(\int_0^{R_m} w^{k+1}(r)rdr - \int_0^{R_p} \psi^{k+1}(\xi)\xi d\xi \right)} \quad (18)$$

that can be simplified as follows:

$$NT^{k+1} = \frac{n\bar{R}T_{Gas}}{V_{Gas}^{(0)} - (\Delta V_m^{k+1} - \Delta V_p^{k+1})} \quad (19)$$

where:

$$\Delta V_m^{k+1} = \Delta V_m^k + \delta(\Delta V_m), \quad \Delta V_p^{k+1} = \Delta V_p^k + \delta(\Delta V_p) \quad (20)$$

$\delta(\Delta V_m)$ and $\delta(\Delta V_p)$ can be found based on the calculus of variations theory as follows:

$$\delta(\Delta V_m) = 2\pi \int_0^{R_m} \delta w r dr = 2\pi \int_0^{R_m} \phi(r)rdr \quad (21)$$

$$\delta(\Delta V_p) = 2\pi \int_0^{R_p} \delta \psi \xi d\xi = 2\pi \int_0^{R_p} \gamma(\xi)\xi d\xi \quad (22)$$

For linearization of the nonlinear term (NT^{k+1}), Taylor's expansion about step k is used as follows:

$$NT^{k+1} = \frac{n\bar{R}T_{Gas}}{V_{Gas}^{(0)} - (\Delta V_m^k - \Delta V_p^k)} + \frac{n\bar{R}T_{Gas}(\Delta V_m^{k+1} - \Delta V_m^k)}{(V_{Gas}^{(0)} - (\Delta V_m^k - \Delta V_p^k))^2} \quad (23)$$

$$- \frac{n\bar{R}T_{Gas}(\Delta V_p^{k+1} - \Delta V_p^k)}{(V_{Gas}^{(0)} - (\Delta V_m^k - \Delta V_p^k))^2} + \dots NT^{k+1} \\ \cong NT^k + \frac{n\bar{R}T_{Gas}\delta(\Delta V_m)}{(V_{Gas}^{(0)} - (\Delta V_m^k - \Delta V_p^k))^2} - \frac{n\bar{R}T_{Gas}\delta(\Delta V_p)}{(V_{Gas}^{(0)} - (\Delta V_m^k - \Delta V_p^k))^2} \quad (24)$$

Similarly, the nonlinear term on the left-hand side of Eq. (16) representing the stretching term can be linearized as follows:

$$N_{am}^{k+1}T(w^{k+1}) = N_{am}^k T(w^k) + N_{am}^k T(\phi(r)) + \delta N_{am} T(w^k) + \delta N_{am} T(\phi(r)) \quad (25)$$

$$N_{ap}^{k+1}T(\psi^{k+1}) = N_{ap}^k T(\psi^k) + N_{ap}^k T(\gamma(\xi)) + \delta N_{ap} T(\psi^k) + \delta N_{ap} T(\gamma(\xi)) \quad (26)$$

For a small change $\Delta \bar{p}_{in}$ in the applied pressure, δN is sufficiently small that the nonlinear terms can be neglected, so that the left-hand-side too can be considered linear.

One more applying the calculus of variations theory, changes in the axial stretching forces are given by:

$$\delta N_{am} = \frac{E_m h_m}{1 - v_m^2} \int_0^{R_m} \left(\frac{\partial w}{\partial r} \right) \Big|_{w=w^k} \left(\frac{\partial \phi}{\partial r} \right) dr \quad (27)$$

$$\delta N_{ap} = \frac{E_p h_p}{1 - v_p^2} \int_0^{R_p} \left(\frac{\partial \psi}{\partial r} \right) \Big|_{\psi=\psi^k} \left(\frac{\partial \gamma}{\partial \xi} \right) d\xi \quad (28)$$

Using a first-order truncation of equation (24) and applying equations (21), (22), (25), (26), (27), and (28) the following system of linear equations is obtained:

$$D_m L(\phi(r)) - (N_{am}^k T(\phi(r) + \delta N_{am} T(w^k))) \\ = -H^{(k)} \int_0^{R_m} \phi(r) r dr + H^{(k)} \int_0^{R_p} \gamma(\xi) \xi d\xi + d\hat{P}_{in} \quad (29)$$

$$D_p L(\gamma(\xi)) - (N_{ap}^k T(\gamma(\xi) + \delta N_{ap} T(\psi^k))) = H^{(k)} \int_0^{R_m} \phi(r) r dr - H^{(k)} \int_0^{R_p} \gamma(\xi) \xi d\xi \quad (30)$$

where H^k is defined as the following form:

$$H^k = \frac{2\pi n\bar{R}T_{Gas}}{(V_{Gas}^{(0)} - (\Delta V_m^k - \Delta V_p^k))^2} \quad (31)$$

There are several methods available to solve the system of boundary value differential equations (29) and (30) such as finite difference and weighted residual methods. In the present paper, the Galerkin weighted residual method is used. In Hilbert Space (Infinite Dimensional

Functions Space) a solution of the bounded differential equations (29) and (30) satisfying the given boundary conditions can be expressed in the form of infinite series in terms of space basis functions

$$\phi(r) = \sum_{i=1}^{\infty} \alpha_{mi} \mu_i(r) \quad , \quad \gamma(\xi) = \sum_{i=1}^{\infty} \alpha_{pi} \Omega_i(\xi) \quad (32)$$

where $\mu_i(r)$ and $\Omega_j(\xi)$ are the basis functions or mode shapes of the membrane and the sensing plate respectively which satisfy the given boundary conditions. According to the Galerkin weighted residual method, the order of the function space can be reduced to a finite number, and the solution can be expressed in the following form:

$$\phi(r) = \sum_{i=1}^N a_{mi} \mu_i(r) \quad , \quad \gamma(\xi) = \sum_{j=1}^M a_{pj} \Omega_j(\xi) \quad (33)$$

Substituting relationships (33) into the system of equations (29) and (30), a linear set of equations is formed as follows:

$$\begin{aligned} & \sum_{i=1}^N D_m L(a_{mi} \mu_i(r)) - N_{am}^k \sum_{i=1}^N T(a_{mi} \mu_i(r)) \\ & - \frac{E_m h_m}{1 - v_m^2} T(w^k) \sum_{i=1}^N a_{mi} \int_0^{R_m} \left(\frac{\partial w}{\partial r} \right) \Big|_{w=w^k} \left(\frac{\partial \mu}{\partial r} \right) dr \\ & = - \sum_{i=1}^N H^k \int_0^{R_m} a_{mi} \mu_i(r) r dr + \sum_{j=1}^M H^k \int_0^{R_p} a_{pj} \Omega_j(\xi) \xi d\xi + \Delta \hat{P}_{in} + \varepsilon_1 \end{aligned} \quad (34)$$

$$\begin{aligned} & \sum_{j=1}^M D_p L(a_{pj} \Omega_j(\xi)) - N_{ap}^k \sum_{j=1}^M T(a_{pj} \Omega_j(\xi)) \\ & - \frac{E_p h_p}{1 - v_p^2} T(\psi^k) \sum_{j=1}^M a_{pj} \int_0^{R_p} \left(\frac{\partial \psi}{\partial \xi} \right) \Big|_{w=w^k} \left(\frac{\partial \Omega}{\partial \xi} \right) d\xi \\ & = - \sum_{i=1}^N H^k \int_0^{R_m} a_{mi} \mu_i(r) r dr + \sum_{j=1}^M H^k \int_0^{R_p} a_{pj} \Omega_j(\xi) \xi d\xi + \varepsilon_2 \end{aligned} \quad (35)$$

here ε_1 and ε_2 , are the errors or residues caused by the reduction in dimension of the function space or Hilbert space. Based on the Galerkin weighted residual method these errors are removed using the following steps. Equation (34) is multiplied into $\mu_{jj}(r)$ and then is integrated over 0 to R_m . Similarly, equation (35) is multiplied into $\Omega_{ii}(\xi)$, and then is integrated over 0 to R_p . Finally, a set of algebraic equations is generated as follows:

$$\begin{aligned}
& \sum_{i=1}^N \int_0^{R_m} D_m \mu_{jj}(r) L(a_{mi} \mu_i(r)) dr - \sum_{i=1}^N \int_0^{R_m} N_{am}^k \mu_{jj}(r) T(a_{mi} \mu_i(r)) dr \\
& - \sum_{i=1}^N \int_0^{R_m} a_{mi} \left(\frac{E_m h_m}{1 - v_m^2} T(w^k) \int_0^{R_m} \left(\frac{\partial w}{\partial r} \right) \Big|_{w=w^k} \left(\frac{\partial \mu}{\partial r} \right) dr \right) dr \\
& = - \sum_{i=1}^N \int_0^{R_m} \mu_{jj}(r) \left(H^k \int_0^{R_m} a_{mi} \mu_i(r) r dr \right) dr \\
& + \sum_{j=1}^M \int_0^{R_m} \mu_{jj}(r) \left(H^k \int_0^{R_p} a_{pj} \Omega_j(\xi) \xi d\xi \right) dr + \int_0^{R_m} \mu_{jj}(r) \Delta \hat{P}_{in} dr
\end{aligned} \tag{36}$$

$$\begin{aligned}
& \sum_{j=1}^M \int_0^{R_p} D_p \Omega_{ii}(\xi) L(a_{pj} \Omega_j(\xi)) d\xi - \sum_{j=1}^M \int_0^{R_p} N_{ap}^k \Omega_{ii}(\xi) T(a_{pj} \Omega_j(\xi)) d\xi \\
& - \sum_{j=1}^M \int_0^{R_p} \Omega_{ii}(\xi) a_{pj} \frac{E_p h_p}{1 - v_p^2} T(\psi^k) \left(\int_0^{R_p} \left(\frac{\partial \psi}{\partial \xi} \right) \Big|_{w=w^k} \left(\frac{\partial \Omega}{\partial \xi} \right) d\xi \right) d\xi \\
& = - \sum_{i=1}^N \int_0^{R_p} \Omega_{ii}(\xi) \left(H^k \int_0^{R_m} a_{mi} \mu_i(r) r dr \right) d\xi \\
& + \sum_{j=1}^M \int_0^{R_p} \Omega_{ii}(\xi) \left(H^k \int_0^{R_p} a_{pj} \Omega_j(\xi) \xi d\xi \right) d\xi
\end{aligned} \tag{37}$$

equations (36) and (37) define a system of linear algebraic equations with $M + N$ unknowns and $M + N$ equations. Solving this set of equations for each step of applying pressure gives the mechanical output of the pressure sensor.

3.1.2 Pressureless State-Related Deflections (Initial Deflections)

Consider figure (1) suppose no pressure is applied yet, two separate states are imaginable for the situation of the pressure sensor in terms of the deflections of the movable parts (membrane and sensing plate). 1) One, the state that the membrane and the sensing plate have no deflections, in other words, the interface volume, V_{Int} , (the total volume of the interface space before filling) completely occupied by silicone oil and the air (e.g., 85 % oil with 15 % air). 2) And one the state that the membrane and sensing plate have a little deflection which is related to incomplete filling of the sensor (e.g., 75 % oil with 15 % air), here the incomplete filling is in terms of the filling the total interface volume. In the present paper, these deflections are called the initial deflections (Note that this naming should not be confused with the dynamic viewpoint, our mean of initial deflections is only related to deflections in the pressureless state). In the case of the existence of the initial deflections for the membrane and plate, the solution procedure is the same as the implemented method, recently. The only difference is related to the initial state (equilibrium state) of the pressure sensor should be determined. At the initial state the volume of air, V_{Gas}^{Eq} , (the volume of air when there is no applied gauge pressure), is calculated as follows:

$$V_{Gas}^{Eq} = V_{Int} - V_{Oil}^{Eq} - \Delta V_{Ini} = V_{Int} - V_{Oil}^{Eq} - 2\pi \left[\int_0^{R_m} w_{Ini}(r)rdr - \int_0^{R_p} \psi_{Ini}(\xi)\xi d\xi \right] \quad (38)$$

where V_{Oil}^{Eq} and ΔV_{Ini} are denote the volume of the silicone oil and the change of the total interface volume due to the initial deflections of the membrane and sensing plate. Because of the incompressibility of the silicone oil the value of V_{Oil}^{Eq} is remained constant while the values of gas volumes depend on the applied pressure and the model parameters. Now suppose that in the presence of the initial deflections, the pressure applies on the membrane, so in this state the volume of the air is given by:

$$V_{Gas} = V_{Gas}^{Eq} - \Delta V = V_{Gas}^{Eq} - 2\pi \left[\int_0^{R_m} w(r)rdr - \int_0^{R_p} \psi(\xi)\xi d\xi \right] \quad (39)$$

where V_{Gas}^{Eq} is given by equation (40). Also, the deflections can be written as:

$$w(r) = w_p^G(r) + w_{Ini}(r) \quad \text{and} \quad \psi(\xi) = \psi_p^G(\xi) + \psi_{Ini}(\xi) \quad (40)$$

where $w_p^G(r)$ and $\psi_p^G(\xi)$ are the membrane and plate deflections caused by the applied gauge pressure, respectively. As we discussed, the principle of the SSL method is based on linearization around a known situation of the system. So, for applying the SSL method to linearization and then using the Galerkin method we need to a known point of the system. Here the equilibrium point is used. The equilibrium point is the state of the pressure sensor where the applied gauge pressure is zero. For the equilibrium state the following system of equations should be solved:

$$D_m \nabla^4 w_{Ini} - \frac{E_m h_m}{1 - \nu_m^2} \left(\frac{1}{2} \int_0^{R_m} \left(\frac{\partial w_{Ini}}{\partial r} \right)^2 dr \right) \nabla^2 w_{Ini} = -\hat{P}_{Gas}^{Eq} + \hat{P}_{atm} \quad (41)$$

$$D_p \nabla^4 \psi_{Ini} - \frac{E_p h_p}{1 - \nu_p^2} \left(\frac{1}{2} \int_0^{R_p} \left(\frac{\partial \psi_{Ini}}{\partial \xi} \right)^2 d\xi \right) \nabla^2 \psi_{Ini} = \hat{P}_{Gas}^{Eq} - \hat{P}_{atm} \quad (42)$$

$$\hat{P}_{Gas}^{Eq} V_{Gas}^{Eq} = n \bar{R} T_{Gas} \quad (43)$$

$$V_{Gas}^{Eq} = V_{Int} - V_{Oil}^{Eq} - 2\pi \left[\int_0^{R_m} w_{Ini}(r)rdr - \int_0^{R_p} \psi_{Ini}(\xi)\xi d\xi \right] \quad (44)$$

where they form 4 equation with 5 unknown parameters (w_{Ini} , ψ_{Ini} , \hat{P}_{Gas}^{Eq} , V_{Gas}^{Eq} and n). Hence, the problem of determining the equilibrium state needs one input. The input for this problem can be considered the volume of the air at the equilibrium state (V_{Gas}^{Eq}). The value of V_{Gas}^{Eq} can be approximated by weighing the pressure sensor assembly via a very sensitive scale. Note that since usually the plate is much stiffer than the membrane, can guess the dominant initial deflection is associates with the membrane.

3.1.3 Determination of the equilibrium state for a given $V_{Gas}^{Eq} = V_{Gas}^*$ and $V_{Oil}^{Eq} = V_{Oil}^*$

At first, note that, since the initial deflections are relatively small (especially for the sensing plate), the stretching terms can be ignored. So, we can write:

$$\left(\frac{\partial w_{Ini}}{\partial r}\right)^2 \cong 0, \quad \left(\frac{\partial \psi_{Ini}}{\partial \xi}\right)^2 \cong 0 \quad (45)$$

By this assumption that the values of the volume of the air and silicone oil at the equilibrium point are known we can guess the solution form as the following function summations:

$$w_{Ini}^*(r) = \sum_{i=1}^M a_i^m f_i(r), \quad \psi_{Ini}^*(\xi) = \sum_{k=1}^N a_k^p g_k(\xi) \quad (46)$$

where the functions $f_i(r)$ and $g_k(\xi)$ are the shape functions of the deflection of the membrane and sensing plate, respectively. Now, by substituting the relationships (46) into differential equations (41), (42), and (44) we can reduce the system to an algebraic system for the unknown coefficients. After substituting, equations (41) and (42) are multiplied into their corresponding shape functions. Integrating over their interval and replacing the parameter \hat{P}_{Gas}^{Eq} from equation (43) into equations (41) and (42) we get the following system of algebraic equations:

$$\begin{aligned} \sum_{i=1}^M A_{ij} a_i^m + q_j^m \hat{P}_{Gas}^{Eq} &= q_j^m \hat{P}_{atm}, \quad j = 1, 2, \dots, M \\ \sum_{k=1}^N B_{kl} a_k^p - q_l^p \hat{P}_{Gas}^{Eq} &= -q_l^p \hat{P}_{atm}, \quad l = 1, 2, \dots, N \\ \sum_{i=1}^M F_i a_i^m - \sum_{k=1}^N G_k a_k^p &= \frac{V_{Int} - (V_{Gas}^* + V_{Oil}^*)}{2\pi} \end{aligned} \quad (47)$$

where:

$$\begin{aligned} A_{ij} &= D_m \int_0^{R_m} f_j(r) \nabla^4 f_i(r) dr, & q_j^m &= \int_0^{R_m} f_j(r) dr, & F_i &= \int_0^{R_m} r f_i(r) dr \\ B_{kl} &= D_p \int_0^{R_p} g_l(\xi) \nabla^4 g_k(\xi) d\xi, & q_l^p &= \int_0^{R_p} g_l(\xi) d\xi, & G_k &= \int_0^{R_p} \xi g_k(\xi) d\xi \\ & & j &= 1, 2, \dots, M \text{ and } l = 1, 2, \dots, N \end{aligned} \quad (48)$$

The system (50) is a set of algebraic equations with $(M + N + 1)$ equations and $(M + N + 1)$ unknown variables (a_i^m s, a_k^p s and \hat{P}_{Gas}^{Eq}). The third equation from the system (51) is the volume-based coupling equation.

3.2 Dynamic Analysis

In the following section, dynamic analysis of the pressure sensor is investigated. For this purpose, equations (9) and (10) should be solved simultaneously. To reduce the system of the non-linear partial differential equations into a lumped model the solution of the system is considered by the following expansions:

$$w(r, t) = \sum_{i=1}^M W_i(t) R_i(r), \quad \psi(\xi, t) = \sum_{l=1}^N \eta_l(t) \Psi_l(\xi) \quad (49)$$

where $R_i(r)$ and $\Psi_l(\xi)$ are the i th and l th mode shapes of the membrane and sensing plate, respectively. Substitution of (49) into equations (9) and (10) and neglecting the stretching terms the following equations will obtain:

$$\begin{aligned} \rho_m h_m \sum_{i=1}^M \ddot{W}_i R_i + C_m \sum_{i=1}^M \dot{W}_i R_i + D_m \sum_{i=1}^M W_i \nabla^4 R_i \\ = - \frac{n \bar{R} T_{gas}}{\pi R_m^2 g_{air} - 2\pi \left(\int_0^{R_m} \sum_{i=1}^M W_i R_i r dr - \int_0^{R_p} \sum_{l=1}^N \eta_l \Psi_l \xi d\xi \right)} + \hat{P}_{in} \\ + \varepsilon_1 \end{aligned} \quad (50)$$

$$\begin{aligned} \rho_p h_p \sum_{l=1}^N \ddot{\eta}_l \Psi_l + C_p \sum_{l=1}^N \dot{\eta}_l \Psi_l + D_p \sum_{l=1}^N \eta_l \nabla^4 \Psi_l \\ = \frac{n \bar{R} T_{gas}}{\pi R_m^2 g_{air} - 2\pi \left(\int_0^{R_m} \sum_{i=1}^M W_i R_i r dr - \int_0^{R_p} \sum_{l=1}^N \eta_l \Psi_l \xi d\xi \right)} - \hat{P}_{atm} \\ + \varepsilon_2 \end{aligned} \quad (51)$$

as before, via Galerkin projection, by multiplying both sides of the equations into their corresponding mode shape then integrating the lumped equations of the model will obtain as follows:

$$\begin{aligned} \sum_{i=1}^M M_{ij}^w \ddot{W}_i + \sum_{l=1}^N C_{ij}^w \dot{W}_i + \sum_{i=1}^M K_{ij}^w W_i \\ = - \int_0^{R_m} \frac{n \bar{R} T_{gas} R_i(r) dr}{\pi R_m^2 g_{air} - 2\pi \left(\int_0^{R_m} \sum_{i=1}^M W_i R_i r dr - \int_0^{R_p} \sum_{l=1}^N \eta_l \Psi_l \xi d\xi \right)} \\ + \bar{P}_j^w \hat{P}_{in}, \quad j = 1, 2, \dots, M \end{aligned} \quad (52)$$

$$\begin{aligned} \sum_{l=1}^N M_{lk}^\psi \ddot{\eta}_l(t) + \sum_{l=1}^N C_{lk}^\psi \dot{\eta}_l + \sum_{l=1}^N K_{lk}^\psi \eta_l(t) \\ = \int_0^{R_p} \frac{n \bar{R} T_{gas} dr \Psi_l(\xi)}{\pi R_m^2 g_{air} - 2\pi \left(\int_0^{R_m} \sum_{i=1}^M W_i R_i r dr - \int_0^{R_p} \sum_{l=1}^N \eta_l \Psi_l \xi d\xi \right)} \\ - \bar{P}_k^\psi \hat{P}_{atm}, \quad k = 1, 2, \dots, N \end{aligned} \quad (53)$$

where:

$$M_{ij}^w = \rho_m h_m \int_0^{R_m} R_j(r) R_i(r) dr, \quad M_{lk}^\psi = \rho_p h_p \int_0^{R_p} \Psi_k(\xi) \Psi_l(\xi) d\xi \quad (54)$$

$$\begin{aligned}
C_{ij}^w &= C_m \int_0^{R_m} R_j(r) R_i(r) dr, & C_{lk}^\psi &= C_p \int_0^{R_p} \Psi_k(\xi) \Psi_l(\xi) d\xi \\
K_{ij}^w &= D_m \int_0^{R_m} R_j(r) \nabla^4 R_i(r) dr, & K_{lk}^\psi &= D_p \int_0^{R_p} \Psi_k(\xi) \nabla^4 \Psi_l(\xi) d\xi \\
\bar{P}_j^w &= \int_0^{R_m} R_j(r) dr, & \bar{P}_k^\psi &= \int_0^{R_p} \Psi_k(\xi) d\xi \\
i, j &= 1, 2, \dots, M, & l, k &= 1, 2, \dots, N
\end{aligned}$$

Based on the geometry of the pressure sensor, an equivalent mechanical lumped model of the pressure sensor is shown in figure (3).

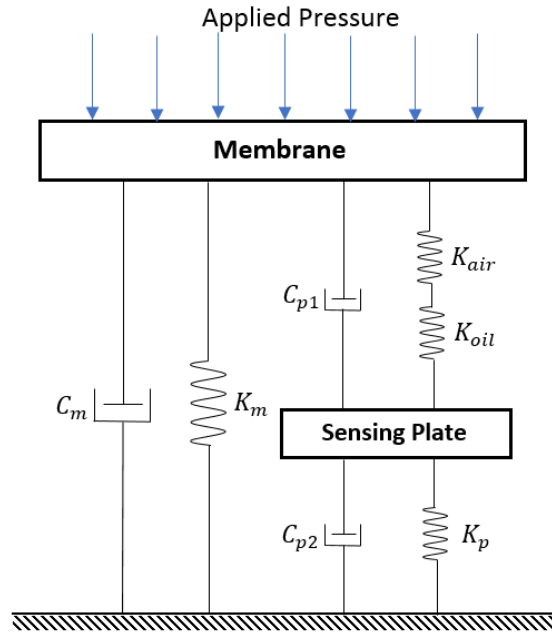


Fig.3: The equivalent mechanical model of the pressure sensor

where K_m , K_p , K_{air} and K_{oil} , are the mechanical stiffness of the membrane, sensing plate, air film, and interface oil respectively. The total stiffness of the system can be calculated as:

$$K_{tot} = K_m + \left(\frac{1}{K_{air}} + \frac{1}{K_{oil}} + \frac{1}{K_p} \right)^{-1} \quad (55)$$

As mentioned, the interface oil is considered to be an incompressible fluid, so that its spring stiffness is infinite and consequently equation (11) can be simplified to:

$$K_{tot} = K_m + \frac{K_{air}K_p}{K_{air} + K_p} \quad (56)$$

Introducing a mechanical equivalent model for the pressure sensor helps to understand how the different components of the pressure sensor respond to the applied input pressure.

4 Numerical Results and Discussion

In this section numerical results are presented based on the previous modeling and solution for the pressure sensor shown in figure (1). Table (1) provides the parameter values used in our example. The main purpose of the present paper is to investigate the influence of trapped air on strain gauge pressure sensors. Accordingly, the sensor output and sensitivity have been determined alongside other key parameters under different conditions and against several effective variables. Note that here sensor output denotes the maximum deflection of the lower plate that in the static analysis it occurs at the center of the plate (displacement of the middle point of the lower plate). Also, the initial deflections are not considered unless mentioned in the text.

Table 1: Characteristics and properties used in numerical analysis.

Geometry parameters		
Membrane radius	R_m	
Middle hole radius	R_h	0.56 mm
Plate radius	R_p	
Thickness of the membrane	h_m	0.038 mm
Thickness of the plate	h_p	0.3 mm
Height of upper cylinder	h_{u0}	0.1 mm
Height of middle cylinder (hole between upper and lower cylinders)	h_h	32 mm
Height of lower cylinder	h_{l0}	0.3 mm
Thickness of air film when no pressure is applied	g_{air}	
Material properties		
Young's modulus of membrane	E_m	205 Gpa
Young's modulus of plate	E_p	205 Gpa
Poisson's ratio of membrane	ν_m	0.3
Poisson's ratio of plate	ν_p	0.3
Universal gas constant	\bar{R}	8.314 J/mol.K

The overall pattern of behavior predicted by simulation studies based on this model is as follows. As the level of air entrainment increases, the membrane (input) movement in response to increasing pressure becomes increasingly non-linear, showing greater movement for the same input pressure. As there are constraints on the maximum displacement, the membrane movement eventually saturates at its maximum value. This input saturation corresponds to a lower input pressure where there is greater air entrainment. The plate (output) movement remains largely linear with respect to input pressure, but increasing membrane sensitivity to air entrainment saturates its output at a lower level.

Consider first the finding that, with air entrainment, the sensor output still responds linearly with the input pressure. This outcome may be explained by the fact that the plate is very much stiffer than the air and the membrane so that the total stiffness of the system and thereby the sensor output is a function of the air and membrane stiffness ($K_{tot} = f(K_m, K_{air})$). Accordingly, the sensing plate only experiences a net pressure, which is the result of the interaction between the membrane and air. It can be seen, however, from figure (4a) that the range of sensor output (i.e., before output saturation occurs) is decreased as the air film

thickness increases (i.e. the percent of the air in the pressure sensor). A possible explanation for this is that the equivalent stiffness of the enclosed air K_{air} is reduced by increasing the air volume. In figure (4b), a similar graph shows the variation of the sensor output with input pressure for various membrane radius, whereby the sensor output rises with increasing membrane radius. Figure (5) shows however that the displacement of the membrane is, with air entrainment, a mildly nonlinear function of input pressure. Increasing air content leads to a decrease in the maximum measurable pressure. Note that the criterion for maximum sensor output is the maximum possible deflection of membrane before fracture or damage in the pressure sensor. This point should be considered during fabrication. This criterion also has been employed for specifying the maximum measurable value by the pressure sensor.

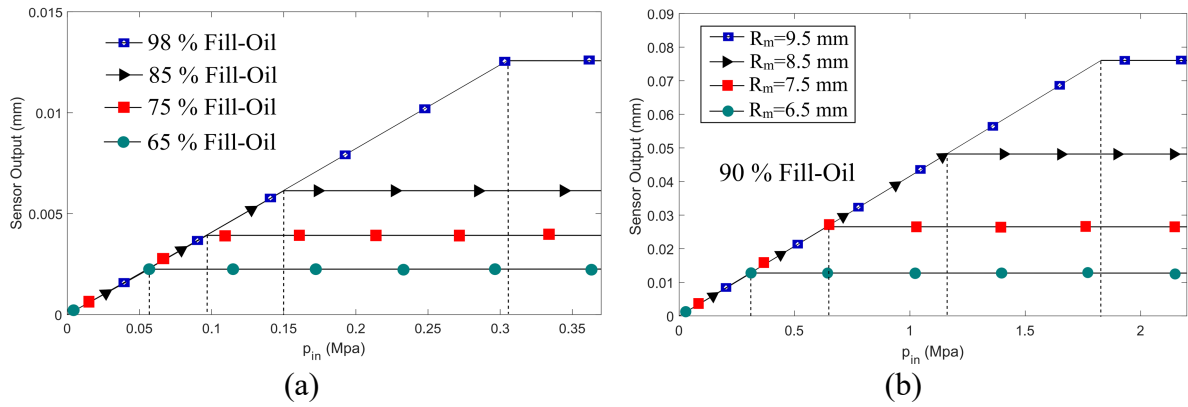
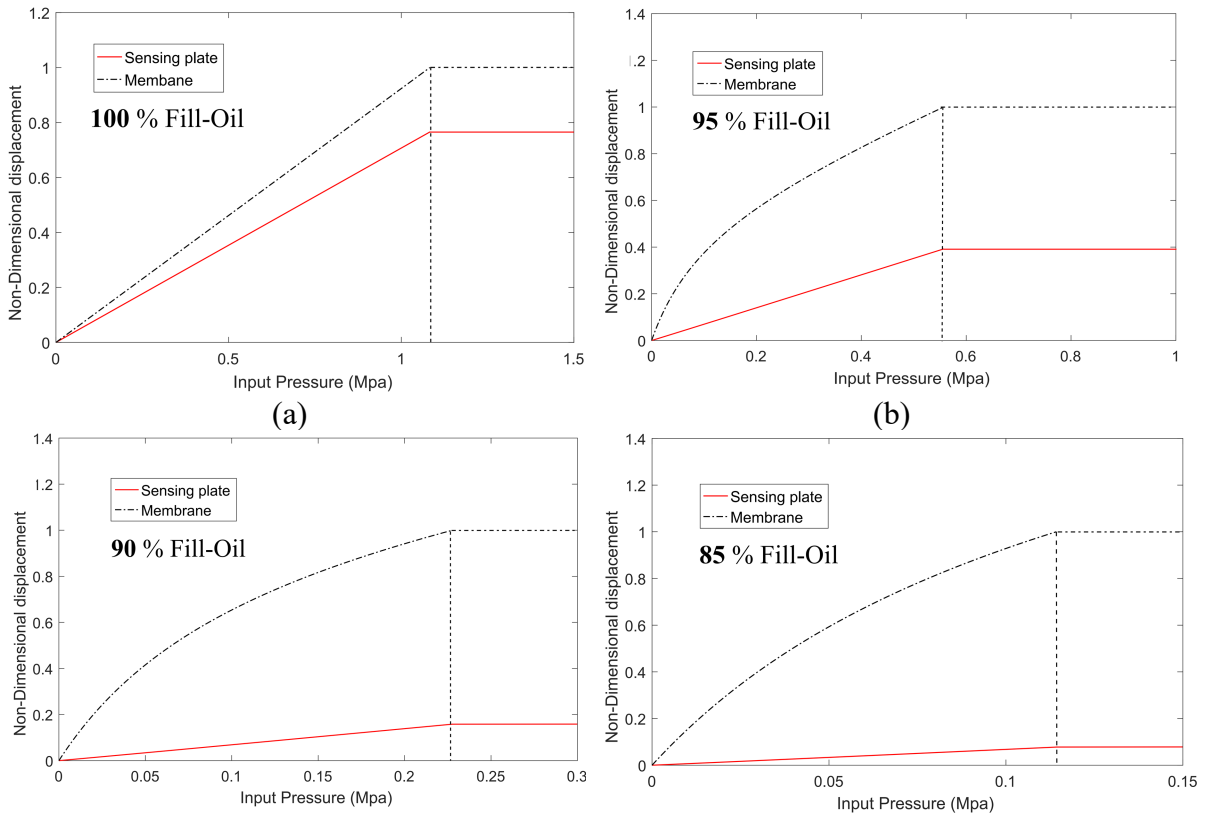


Fig.4: Variations of the sensor output versus input pressure for a) different percentages of fill-Oil b) different membrane radius. The straight line indicates no change in sensor output for higher pressures corresponding to each mode



(c)

(d)

Fig.5: Non-dimensional displacement of the membrane and sensing plate as a function of the input pressure for a) nonfaulty pressure sensor b) with 95 percentages fill-oil c) with 90 percentages fill-oil d) with 85 percentages fill-oil.

Where the stiffness of the plate is not much more than that of the membrane and air, some nonlinearity is observed in the sensor output and which requires a few correction factors to accurate calibrate and linearize the output signal. With the low stiffness of the sensing plate, the range of measurable pressure by the sensor is severely restricted, so it is better for the plate to be stiffer than the membrane and air.

As stated previously, the maximum measurable pressure in such sensors is restricted by the maximum deflection of the membrane. For the geometry of the pressure sensor shown in Figure 2, the maximum deflection of the membrane is h_{u0} . Of course, the value of the h_{u0} is determined by the elasticity limitation of the membrane. Once the maximum deflection of the membrane is reached, the pressure sensor saturates at its maximum obtainable output. The relationship between maximum measurable pressure (MMP), and percent of fill-oil and membrane radius, are shown in figures (6) and (7) respectively. These results are based on the parameter values given in Table 1.

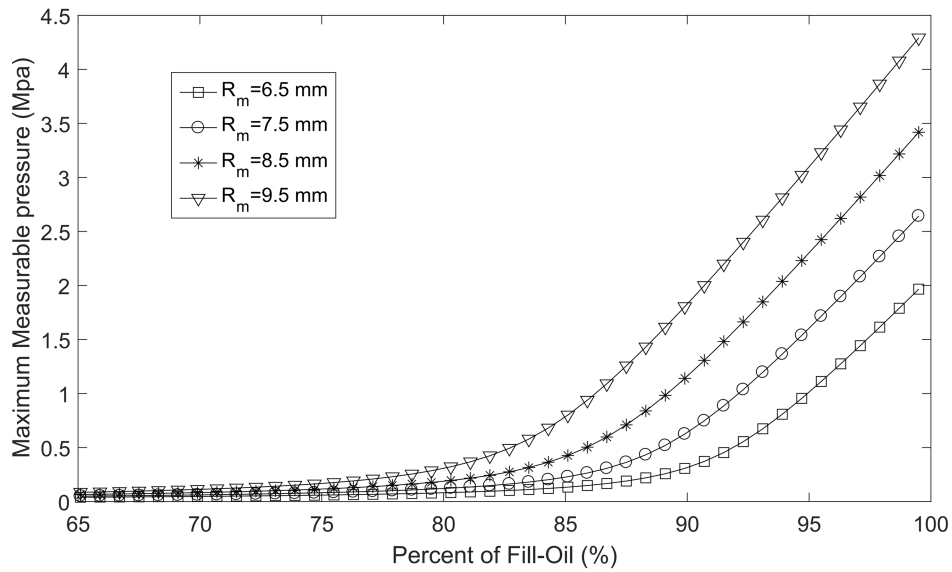


Fig.6: Variations of the maximum measurable pressure as a function of the value of the percent of filler-oil for various membrane radius

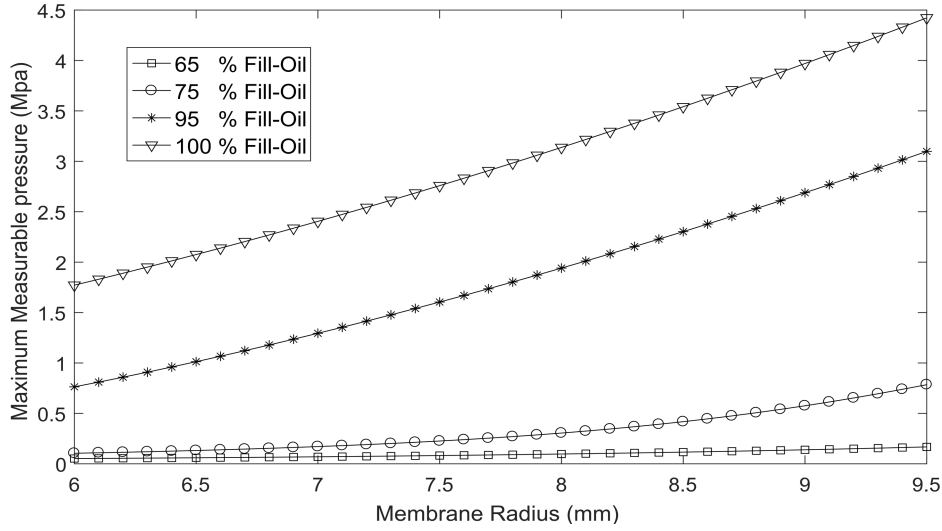


Fig.7: Variations of the maximum measurable pressure as a function of the membrane radius for different oil percentages

As can be seen in figures (6) and (7), the MMP rises with increasing the percentage of the filler Oil (decreasing the equivalent air film thickness), as well as increases with increasing the membrane radius. Another important conclusion from figures (6) and (7) is that beyond a certain value of the air percent, the MMP is not a function of the membrane radius.

One of the most important parameters in determining the accuracy and the effectiveness of the pressure sensors is sensitivity, and it is introduced as $S = \Delta X / \Delta P$ where S , is sensitivity, P is the input pressure and X denotes the output signal [25]. This definition gives a good indication of the impact of the effective parameters on the sensitivity of the pressure sensor and assists designers in choosing optimum geometrical and material parameters. Based on the definition (39) the variations of the sensitivity relative to the membrane radius and air film thickness have been computed and the results are summarized in figures (8) and (9).

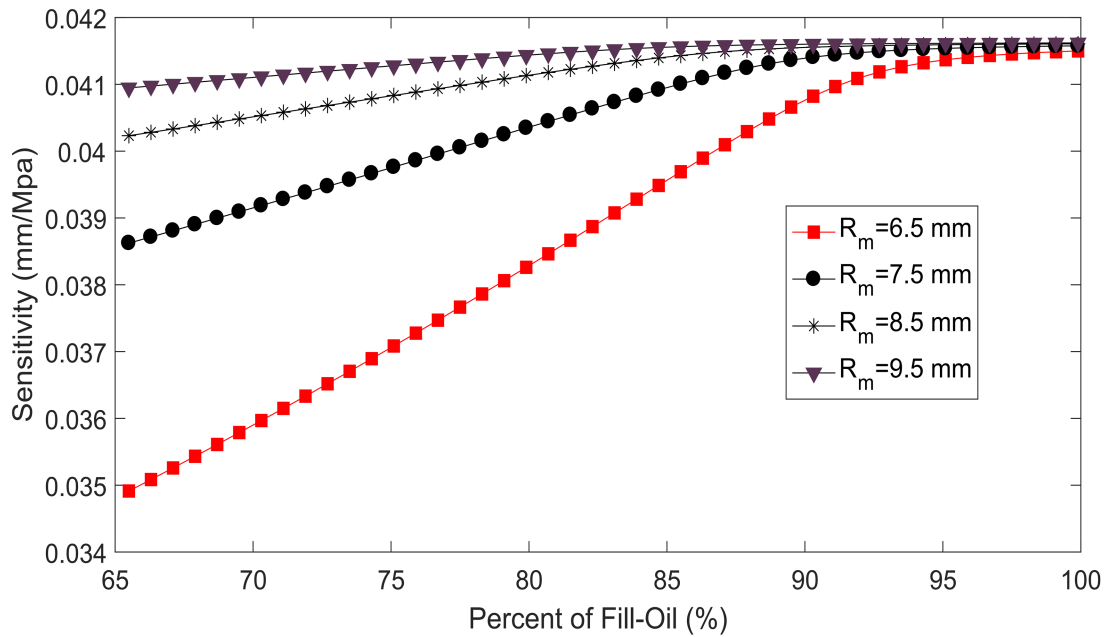


Fig.8: The sensitivity of the pressure sensor versus percent of filler oil under different states of the membrane radius

As shown in figure (8) the sensitivity is increased by increasing the filler oil. So, preventing air or gas entrainment can maintain the functionality of the pressure sensor. Figure (9) shows the variations of the sensitivity of the pressure sensor as a function of the membrane radius. Increasing the radius of the membrane gives increased sensitivity.

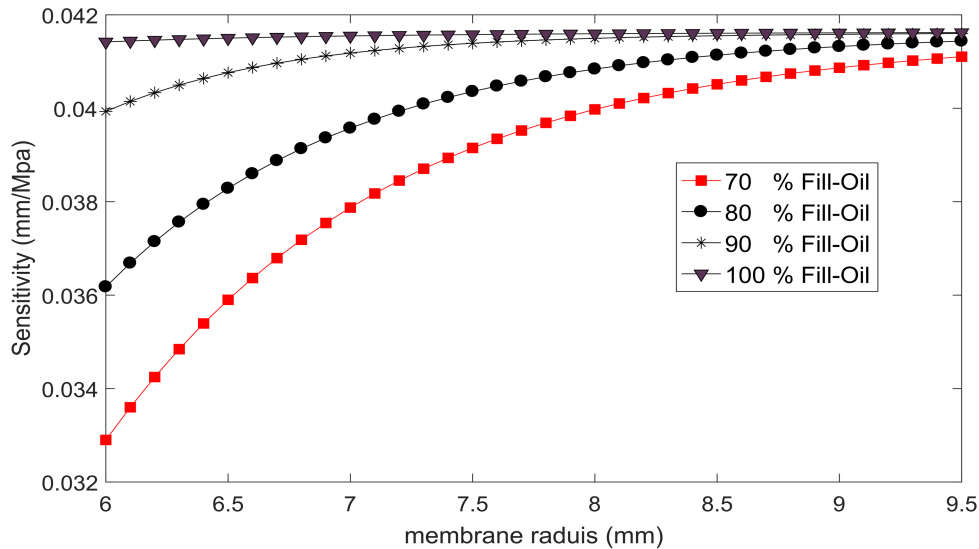


Fig.9: Relationship between the sensitivity and the membrane radius at different air film.

Finally, the effects of the (steady) operating temperature are derived. According to the simulated results shown in figure (10), the variation of the temperature has low effect on the functionality of the pressure sensor.

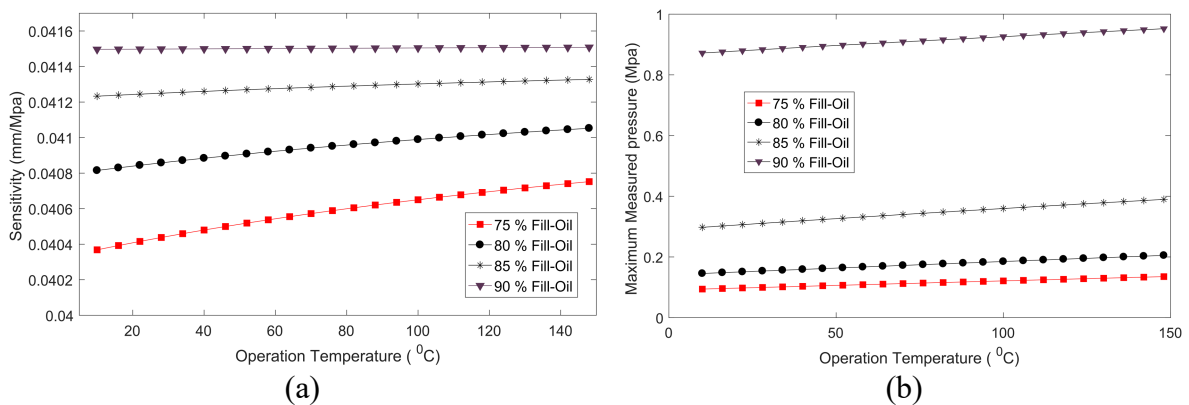


Fig 10: The variations of the a) sensitivity and b) maximum measurable pressure relative to the operating temperature at different air film thicknesses. The above graphs are extracted by assuming the $R_m = 8 \text{ mm}$.

So far, in the result sections was supposed the movable parts of the pressure sensor have no initial deflections due to incomplete filling of interface volume. In continuation, the effects of the initial deflections on the sensor performance will be investigated. The membrane deflection and the sensor output as a function of input gauge pressure are shown in figure (11). According to figure (11), can be concluded that the MMP for the pressure sensor movable components is reduced respect to the state that the sensor has no initial deflection. Table (2) compares the amount of change of the MMP and sensitivity for different state of filling of the pressure sensor

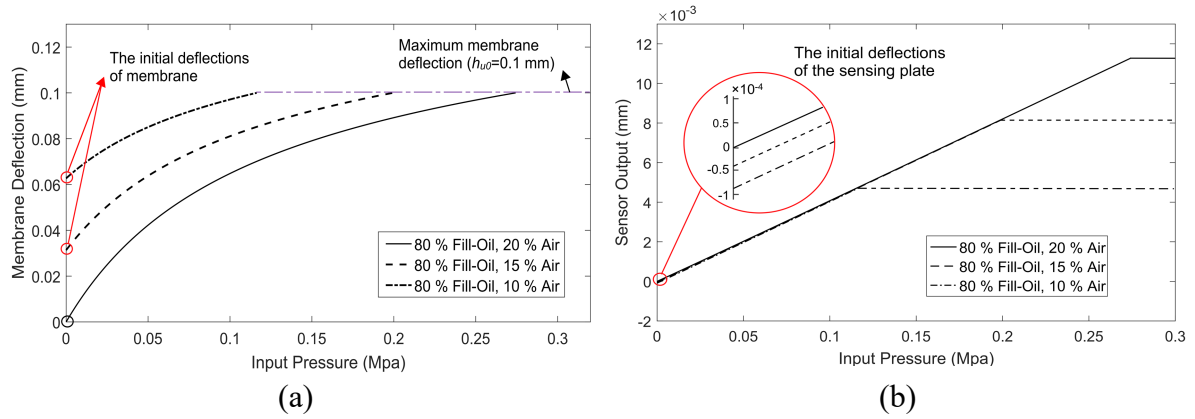


Fig.11: The deflection versus input pressure for a) the membrane and b) the sensing plate in three cases of filling of the sensor.

Table 2: The maximum pressure measured by the sensor for different states of filling.

Filling state	80% Oil + 20% Air	80% Oil + 15% Air	80% Oil + 10% Air	80% Oil + 5% Air
MMP (Pa)	2.743×10^5	1.994×10^5	1.163×10^5	0.204×10^5
Sensitivity (mm/Mpa)	0.0411	0.0409	0.0404	0.0348

Dynamic analysis of the sensor is carried out to investigate the general response of the sensor to a step external pressure. The damping coefficients have been applied to model energy dissipation factors such as external air on the sensing plate or the viscous damping of the pressure line for example when the pressure sensor has installed on a pipe. As figure (12-a) shows the oil insufficiency can significantly influence the membrane deflection, whereas, the sensor output or plate deflection does not change much in the steady-state response, this result completely agrees with the static analysis earlier. Therefore, the MMP by the sensor is restricted due to the allowable deflection of the membrane.

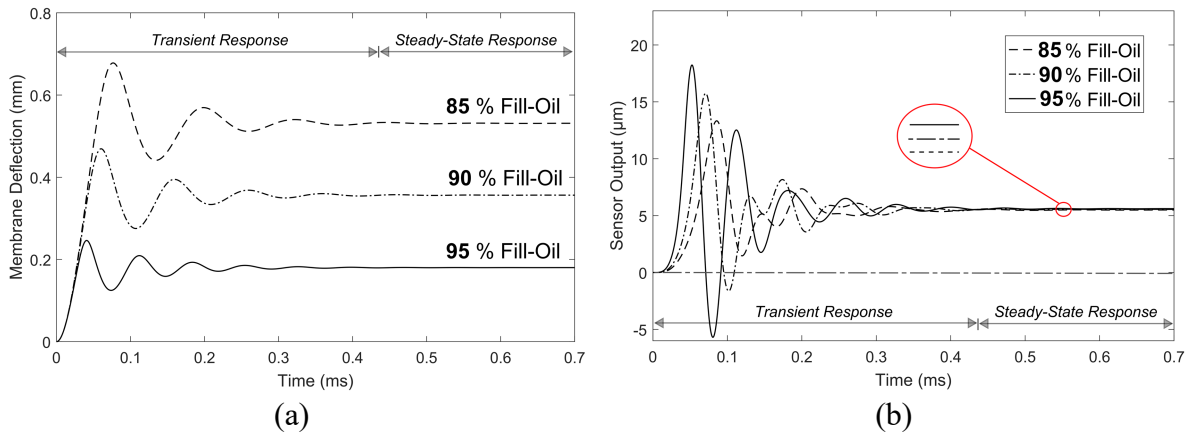


Fig.12: The time history of the system for a) the membrane and b) the sensing plate in three cases of filling of the sensor ($P_{in} = 0.24 \text{ Mpa}$, $R_m = 9.5 \text{ mm}$, $R_p = 6 \text{ mm}$).

5 Conclusion

In the current article insufficiency of the interface oil on the static and dynamic performance of a strain gauge type pressure sensor was studied. The governing deflection equations of the membrane and the sensing plate of the sensor were derived based on Kirchhoff's thin plate theory considering mid-plane stretching. The air trapped in the space between the two plates was modeled as a polytropic gas and the oil is considered as an incompressible fluid. In the static analysis, the coupled nonlinear differential equations were solved using a step-by-step linearization method and the obtained linearized equations at each step were discretized based on a Galerkin reduced-order model. For the dynamic model also after reducing the equations into an equivalent lumped model, the numerical integration method based on the 4th-order Runge-Kutta method was used. Solving the governing equations, the initial deflections of the membrane and the sensing plate in the static form when there is no applied external pressure for different oil value insufficiencies were calculated. Also, the deflection of the membrane, the sensing plate as sensor output, and maximum measurable pressure (MMP) for different values of the interface oil and the trapped air were determined and was compared with the nonfaulty sensor. It was shown that with increasing the trapped air the measurable pressure decreases, however as the stiffness of the membrane in comparison to the stiffness of the sensing plate is too low the sensor output remains without changes. Besides the effect of initial deflection on the sensor performance was examined and it was shown that it does not affect sensor output and it also as same as oil insufficiency only decreases maximum measurable pressure. The dynamical response of the sensor verified the results of the static analysis in terms of the behavior of the system in the steady-state response. The effect of some geometrical parameters such as the membrane radius on the sensor performance was studied and shown that increasing its value increases sensor sensitivity but decreases the measurable range of the pressure. The obtained results can be useful for the sensor and instrumentation community in designing strain gauge type pressure sensors.

Compliance with ethical standards

Conflict of interest: The authors declare that there is no conflict of interests regarding the publication of the paper.

References

- [1] M. M. Nayak, N. Gunasekaran, K. Rajanna, S. Srinivasulu, and S. Mohan, "The Strain Gauge Pressure Transducers—An Overview," *IETE Tech. Rev.*, vol. 9, no. 2, pp. 170–177, Mar. 1992, doi: 10.1080/02564602.1992.11438858.
- [2] E. G. Bakhoun and M. H. M. Cheng, "Capacitive pressure sensor with very large dynamic range," *IEEE Trans. Components Packag. Technol.*, vol. 33, no. 1, pp. 79–83, 2009.
- [3] J. Yang, Y. Ye, X. Li, X. Lü, and R. Chen, "Flexible, conductive, and highly pressure-sensitive graphene-polyimide foam for pressure sensor application," *Compos. Sci. Technol.*, vol. 164, pp. 187–194, 2018, doi: 10.1016/j.compscitech.2018.05.044.
- [4] J. Tabor *et al.*, "Textile-based Pressure Sensors for Monitoring Prosthetic-Socket Interfaces," *IEEE Sens. J.*, p. 1, 2021, doi: 10.1109/JSEN.2021.3053434.
- [5] D. Tandeske, "Pressure sensors: Selection and Application, New York: M." Dekker,

1991.

- [6] S. S. Kumar and B. D. Pant, "Erratum to: Design principles and considerations for the 'ideal' silicon piezoresistive pressure sensor: a focused review," *Microsyst. Technol.*, vol. 20, no. 12, pp. 2303–2303, Dec. 2014, doi: 10.1007/s00542-014-2289-2.
- [7] A. Z. Hajjaj, N. Alcheikh, M. A. A. Hafiz, S. Ilyas, and M. I. Younis, "A scalable pressure sensor based on an electrothermally and electrostatically operated resonator," *Appl. Phys. Lett.*, vol. 111, no. 22, 2017, doi: 10.1063/1.5003563.
- [8] A. Bouchaala *et al.*, "Nonlinear-based MEMS sensors and active switches for gas detection," *Sensors (Switzerland)*, vol. 16, no. 6, 2016, doi: 10.3390/s16060758.
- [9] T. Xu *et al.*, "A high sensitive pressure sensor with the novel bossed diaphragm combined with peninsula-island structure," *Sensors Actuators A Phys.*, vol. 244, pp. 66–76, Jun. 2016, doi: 10.1016/j.sna.2016.04.027.
- [10] K. Soltani, E. Tugova, M. P. Henry, O. Bushuev, M. Ghanbari, and G. Rezazadeh, "Modelling Fluid Loss Faults in an Industrial Pressure Sensor," in *Proceedings - 2020 Global Smart Industry Conference, GloSIC 2020*, 2020, pp. 215–222, doi: 10.1109/GloSIC50886.2020.9267837.
- [11] S. Luo *et al.*, "Tunable-Sensitivity flexible pressure sensor based on graphene transparent electrode," *Solid. State. Electron.*, vol. 145, pp. 29–33, Jul. 2018, doi: 10.1016/j.sse.2018.04.003.
- [12] P. Song *et al.*, "Recent progress of miniature MEMS pressure sensors," *Micromachines*, vol. 11, no. 1, pp. 1–38, 2020, doi: 10.3390/mi11010056.
- [13] D. J. Young, J. Du, C. A. Zorman, and W. H. Ko, "High-temperature single-crystal 3C-SiC capacitive pressure sensor," *IEEE Sens. J.*, vol. 4, no. 4, pp. 464–470, 2004, doi: 10.1109/JSEN.2004.830301.
- [14] Y. Yang *et al.*, "Flexible piezoelectric pressure sensor based on polydopamine-modified BaTiO₃/PVDF composite film for human motion monitoring," *Sensors Actuators A Phys.*, vol. 301, p. 111789, Jan. 2020, doi: 10.1016/j.sna.2019.111789.
- [15] Y. Seo, D. Kim, and N. A. Hall, "High-Temperature Piezoelectric Pressure Sensors for Hypersonic Flow Measurements," in *2019 20th International Conference on Solid-State Sensors, Actuators and Microsystems & Eurosensors XXXIII (TRANSDUCERS & EUROSENSORS XXXIII)*, Jun. 2019, vol. 28, no. 2, pp. 2110–2113, doi: 10.1109/TRANSDUCERS.2019.8808755.
- [16] H. H. Tsai, C. C. Hsieh, C. W. Fan, Y. C. Chen, and W. Te Wu, "Design and characterization of temperature-robust piezoresistive micro-pressure sensor with double-wheatstone-bridge structure," in *DTIP of MEMS and MOEMS - Symposium on Design, Test, Integration and Packaging of MEMS/MOEMS*, 2009, pp. 363–368.
- [17] B. R. Burg, T. Helbling, C. Hierold, and D. Poulikakos, "Piezoresistive pressure sensors with parallel integration of individual single-walled carbon nanotubes," *J. Appl. Phys.*, vol. 109, no. 6, p. 064310, Mar. 2011, doi: 10.1063/1.3555619.
- [18] Shuang Chen, Ming-quan Zhu, Bing-he Ma, and Wei-zheng Yuan, "Design and optimization of a micro piezoresistive pressure sensor," in *2008 3rd IEEE International Conference on Nano/Micro Engineered and Molecular Systems*, 2008, pp. 351–356, doi: 10.1109/NEMS.2008.4484350.

- [19] J. Ji *et al.*, “An ultraminiature CMOS pressure sensor for a multiplexed cardiovascular catheter,” *IEEE Trans. Electron Devices*, vol. 39, no. 10, pp. 2260–2267, 1992, doi: 10.1109/16.158797.
- [20] Y.-H. Zhang, C. Yang, Z.-H. Zhang, H.-W. Lin, L.-T. Liu, and T.-L. Ren, “A Novel Pressure Microsensor With 30- μm -Thick Diaphragm and Meander-Shaped Piezoresistors Partially Distributed on High-Stress Bulk Silicon Region,” *IEEE Sens. J.*, vol. 7, no. 12, pp. 1742–1748, Dec. 2007, doi: 10.1109/JSEN.2007.910298.
- [21] A. A. Barlian, W.-T. Park, J. R. Mallon, A. J. Rastegar, and B. L. Pruitt, “Review: Semiconductor Piezoresistance for Microsystems.,” *Proc. IEEE. Inst. Electr. Electron. Eng.*, vol. 97, no. 3, pp. 513–552, Mar. 2009, doi: 10.1109/JPROC.2009.2013612.
- [22] S. S. Rao, *Vibration of Continuous Systems*, vol. 464. Hoboken, NJ, USA: John Wiley & Sons, Inc., 2006.
- [23] M. B. Moran, Michael J.; Shapiro, Howard N.; Boettner, Daisie D.; Bailey, *Fundamentals of Engineering Thermodynamics*. CRC Press, 2019.
- [24] G. Rezazadeh, A. Tahmasebi, and M. Zubstov, “Application of piezoelectric layers in electrostatic MEM actuators: controlling of pull-in voltage,” *Microsyst. Technol.*, vol. 12, no. 12, pp. 1163–1170, Oct. 2006, doi: 10.1007/s00542-006-0245-5.
- [25] Y. Zang, F. Zhang, C. Di, and D. Zhu, “Advances of flexible pressure sensors toward artificial intelligence and health care applications,” *Mater. Horizons*, vol. 2, no. 2, pp. 140–156, 2015, doi: 10.1039/C4MH00147H.